Neuron, Vol. 14, 763–771, April, 1995, Copyright © 1995 by Cell Press

Growth Cone Advance Is Inversely Proportional to Retrograde F-Actin Flow

Chi-Hung Lin and Paul Forscher
Department of Biology
Yale University
New Haven, Connecticut 06520

Summary

In a previous study, F-actin appeared to play a key role in guiding microtubules during growth cone–target interactions. Here, F-actin flow patterns were assessed to investigate the relationship among F-actin flow, microtubule/organelle protrusion, and rates of outgrowth. We first demonstrated conditions in which surface markers (beads) moved at the same rate as underlying F-actin. These beads were then positioned, using laser tweezers, to assess F-actin movements during target interactions. We found retrograde F-actin flow was attenuated specifically along the target interaction axis in direct proportion to the rate of growth cone advance. Retrograde actin flow adjacent to the interaction axis was unperturbed. Our results suggest that growth cones transduce retrograde F-actin flux into forward movement by modulating F-actin–substrate coupling efficiency.

Introduction

Pathfinding decisions during axonal outgrowth in developing and regenerating neurons are largely attributed to a specialized structure at the distal end of the neurite called the growth cone. Neuronal growth cones can direct neurite outgrowth physically by recognizing and interpreting extracellular molecular cues, which they respond to with changes in structure and motility (Burmeister et. al., 1991; Heidemann et al., 1991; Cypher and Letourneau, 1992; Lander, 1992; Goodman and Shatz, 1993; Hatten, 1993; O'Leary and Koester, 1993; Letourneau et al., 1994). Although modulation of growth cone motility is thought to be mediated through regulation of intracellular cytoskeletal and associated motor proteins, the cytomechanical basis of these events has not been well characterized. Aplysia bag cell neuron growth cones have been shown previously to interact with growth cones or neurites from neighboring bag cells (Lin and Forscher, 1993) and eventually form gap junctions in culture (Kaczmarek et al., 1979), thus providing a simple, well controlled system for investigating basic mechanisms of neuronal interaction.

Recent studies of cytoskeletal dynamics during growth cone–target interactions suggested a specific role for actin-based motility in axonal guidance processes (Lin and Forscher, 1993; O'Connor and Bentley, 1993; Smith, 1994). Under control conditions in isolated growth cones, F-actin networks are preferentially assembled at the leading margin, then move centripetally at flow rates of 3–6 μm/min (Forscher and Smith, 1988). Our recent observations of growth cone behavior during target recognition events suggested these F-actin networks could play a key role in directing microtubule movements and microtubule-associated organelles (Lin and Forscher, 1993). We noted that retrograde F-actin flow seemed to be perturbed during growth cone–target interactions; specifically, rates of central domain extension and retrograde F-actin flow appeared to be inversely related. Here, we have directly tested this hypothesis by mapping F-actin flow and organelle/microtubule redistribution during growth cone–target interactions.

We first determined experimental conditions whereby surface markers (polycationic microbeads) were physically coupled to underlying actin networks and thus moved in synchrony with the retrograde F-actin flow (Forscher and Smith, 1990). Such beads could then be used as tools to monitor noninvasively intracellular F-actin movements (Forscher and Smith, 1988). Then, by employing an infrared single-beam gradient optical trap (laser tweezers; Block, 1990) to position beads rapidly on the growth cone surface during target interactions, we generated a map of F-actin flow patterns throughout the lamella. We found that the retrograde flow was attenuated specifically along the target interaction axis, where the central domain (and associated microtubules) preferentially extended toward the target. In addition, slowing of the retrograde flow was proportional to the observed rates of growth cone advance. These results suggest a simple mechanism by which growth cones regulate the rate and direction of axonal growth by varying the degree of physical coupling between intracellular F-actin networks and external target substrates.

Results

Growth Cone–Target Interactions

A typical in vitro growth cone–target interaction sequence is shown in Figure 1. Note stretching of individual filopodia at the beginning of the interaction (arrowhead in Figure 1A), and preferential extension of central cytoplasmic domain toward the site of interaction over time (arrow in Figure 1A, 5'). After this initial phase, a growth cone would typically turn and migrate along the surface of the companion neuron (arrows in Figure 1A, 30' and 50') at rates about 10 times faster than those observed prior to the interaction. Cumulative displacement of the leading edge and central domain for the growth cone on the right is shown in Figure 1B. Although the leading edge initially appeared to increase its rate of advance more slowly than the central domain (Figure 1B, dashed window) both structures advanced at similar rates after the acute phase (~10 min) of the interaction. Since the distal boundary of the central cytoplasmic domain could be located with greater precision than the ruffling leading edge, displacement of the central domain was typically used to assess rates of growth cone advance (see Figure 7 and Discussion). Cytoskeletal organization after a typical growth cone–growth cone interaction is shown in Figure 1C. Note F-actin accumulation at the site of interaction (Figure 1C) and microtu-

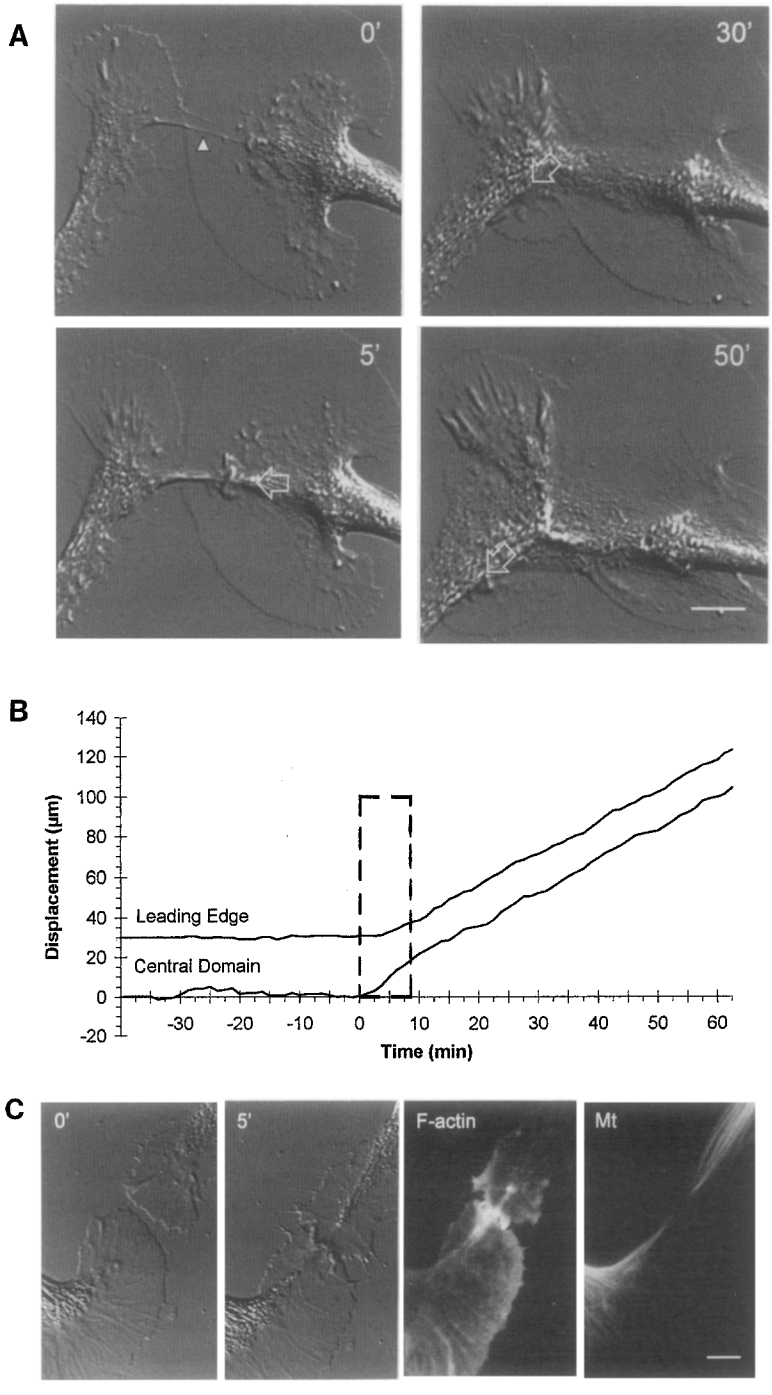

Figure 1. Typical Structural and Cytoskeletal Dynamics during Homophilic Aplysia Growth Cone–Growth Cone Interactions

(A) Video-enhanced differential interference contrast (DIC) image sequence of a growth cone–growth cone interaction. Filopodium stretching (arrowhead, 0') occurred at the beginning of the interaction. After 5 min, the central domain had extended to the target contact site (open arrow, 5'). The growth cone then turned and migrated downward along the neurite of the companion neuron (open arrows, 30' and 50') at a rate of 1.2 μm/min, about ten times faster than the advance rate before the interaction (Lin and Forscher, 1993).

(B) Cumulative displacements of the leading edge and the central domain of the growth cone on the right in (A) plotted as a function of time. Time zero marks the initiation of the central domain extension (or the start of the interaction; see Lin and Forscher, 1993). Note that the leading edge and the central domain advanced in parallel, except during the initial phase (dashed line) of target interaction.

(C) Typical cytoskeletal reorganization during growth cone–growth cone interactions. Intracellular actin filaments (F-actin) and microtubules (Mt) are visualized with rhodamine-phalloidin or β-tubulin immunofluorescence, respectively. Note that extension of the central cytoplasmic domain coincides with target site-directed microtubule elongation. Time is in minutes; bar, 10 μm.

bule extension along the growth cone–target interaction axis coinciding with the protrusion of the central cytoplasmic domain (Figure 1C; for details, see Lin and Forscher, 1993). The observation that the target site-directed microtubule extension depicted in Figure 1C could be randomized by cytochalasin treatment (Lin and Forscher, 1993) suggested a key role for F-actin dynamics in directing microtubule reorganization.

Surface Marker Movement Reflects Underlying F-Actin Flow

To construct a spatial map of actin flow patterns before and during interactions, we first determined experimental conditions under which membrane-bound polycationic beads moved in precise synchrony with the underlying F-actin flow. We used fluorescence photobleaching techniques to characterize F-actin dynamics (Wang, 1985, 1987; O'kabe and Hirokawa, 1991), using either microinjected rhodamine-phalloidin (RH-ph) or rhodamine-labeled G-actin (RH-actin) to label the intracellular actin cytoskeleton. Similar results were obtained by both methods.

To determine whether both of the injected fluorescent probes labeled the entire actin filament population in growth cones, labeling patterns of injected RH-ph (Figure

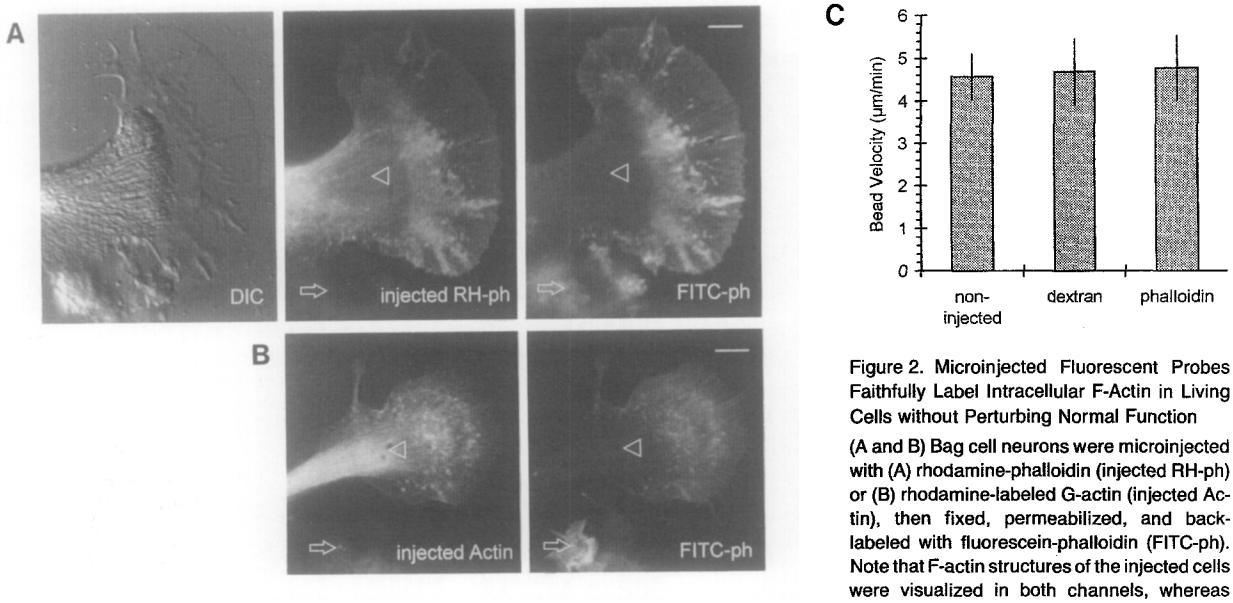

Figure 2. Microinjected Fluorescent Probes Faithfully Label Intracellular F-Actin in Living Cells without Perturbing Normal Function

(A and B) Bag cell neurons were microinjected with (A) rhodamine-phalloidin (injected RH-ph) or (B) rhodamine-labeled G-actin (injected Actin), then fixed, permeabilized, and back-labeled with fluorescein-phalloidin (FITC-ph). Note that F-actin structures of the injected cells were visualized in both channels, whereas neighboring noninjected glial cells were labeled only by postfixation–extraction labeling (arrows; weak signal in rhodamine channel is likely due to low levels of autofluorescence). Bar, 10 μm.

(C) Labeling procedures do not affect functional integrity of retrograde F-actin flow assessed by surface marker movements. Bead transport rates for phalloidin-injected growth cones were comparable with those observed in noninjected cells or cells microinjected with 43 kDa rhodamine-dextran.

2A) or RH-actin (Figure 2B) were compared with fluorescein isothiocyanate–phalloidin (FITC-ph) staining after fixation and extraction in the same cells. The two labeling protocols revealed essentially the same patterns of F-actin structure in peripheral lamellar domains, and neither was significantly different from F-actin patterns typically observed in noninjected cells (Forscher and Smith, 1988; Lin and Forscher, 1993) or control cells injected with inert fluorescent molecules such as rhodamine-dextran (data not shown). In RH-ph or RH-actin injected cells, we also observed fluorescent labeling in proximal growth cone regions (arrowheads in Figures 2A and 2B) and along neurites. It is likely that this labeling represents either fluorescent probe molecules in the cytoplasm or cortical-actin cytoskeleton, since labeling in these regions was sensitive to detergent extraction and exhibited only weak staining with FITC-ph after fixation (arrowheads in Figures 2A and 2B, FITC-ph). Note that neighboring noninjected glial cells (arrows in Figures 2A and 2B) exhibited clear F-actin labeling with FITC-ph and only weak background fluorescence in the rhodamine (injected probe) channel. To test whether these actin labeling procedures adversely affected lamellipodial dynamics, we measured translocation rates of membrane-bound beads before and after microinjection. As shown in Figure 2C, bead transport rates for growth cones injected with phalloidin (4.78 ± 0.76 μm/min; n = 136 beads from 10 cells) were comparable with those observed in noninjected cells (4.57 ± 0.54 μm/min; n = 198 beads from 14 cells) or cells microinjected with rhodamine-dextran (4.69 ± 0.77 μm/min, n = 99 beads from 10 cells), suggesting that the structural and functional integrity of the actin matrix was maintained after actin labeling.

After fluorescent probes had incorporated into F-actin networks, positively charged beads were applied to the growth cones together with bovine serum albumin in the medium to prevent possible site-directed actin assembly induced by bead binding (Forscher et al., 1992; see Experimental Procedures). F-actin was rapidly marked by repeated high power laser line scans near the bead attachment site; then bead and F-actin movements were simultaneously recorded using dual channel confocal microscopy. As shown in Figure 3A, bead (arrowheads) and photobleached mark (arrows) displacements during a 10 s observation interval were the same, using RH-ph as a fluorescent F-actin probe. Similar results were obtained using growth cones injected with RH-actin. Figure 3B shows the position of the initial mark on a growth cone injected with RH-actin (top) and a time sequence of simultaneous fluorescent actin (bottom left) and bead (bottom right) images. To confirm that actin and beads were moving in parallel, bead positions from the differential interference contrast (DIC) images were superimposed on corresponding fluorescent F-actin images (Figure 3C, left). Finally, to determine the position of photobleached marks accurately, fluorescence intensity line scans perpendicular to the marks were plotted as a function of distance for different time points after photobleaching. The positions of photobleached marks are readily discernible as abrupt negative deflections in the line intensity scans. Comparison of these negative deflections and corresponding bead centroid positions (Figure 3C, open circles) indicated that beads were moving at the same speed as underlying F-actin (4.46 ± 2.13 μm/min, mean ± SD; n = 15 photobleaching experiments). Note the gradual increase of distal to proximal

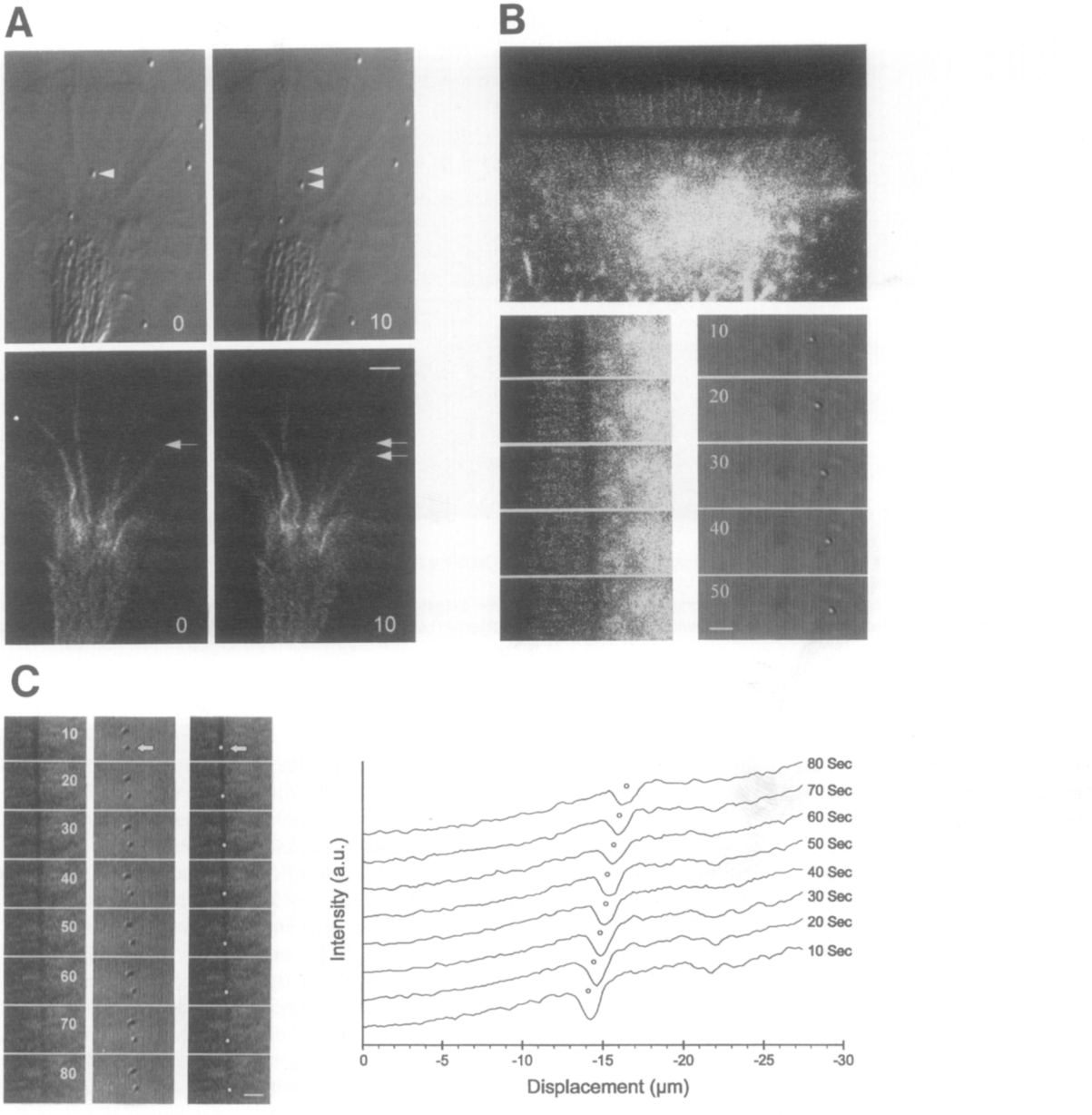

Figure 3. Flow-Coupled Beads on the Growth Cone Membrane Surface Move at the Same Speed as Underlying F-Actin Networks

Photobleaching experiments were performed on RH-ph-injected (A) or RH-actin-injected (B) growth cones, and simultaneous fluorescent and DIC confocal images were taken to correlate surface particle and F-actin movement.

(A) In RH-ph-injected cells, the bead displacement in a 10 s interval (arrowheads) was essentially identical to the movement of photobleached marks (arrows indicate proximal margin of marks).

(B) In a RH-actin-injected growth cone, a photobleached mark was generated using high power line scans (top). Image sequence of simultaneous fluorescent (bottom left) and DIC (bottom right) shows synchronized movements of beads and photobleached marks. Time (in seconds) after photobleaching is indicated.

(C) To analyze bead and bleached mark movement, bead positions in a RH-ph-injected growth cone were superimposed on photobleached marks to verify synchronized movement (left). Fluorescence intensity scans (right) were made normal to photobleached marks and plotted as a function of displacement (negative numbers indicate retrograde direction) for each time point. Negative deflections in line scans denote photobleached marks; open circles denote bead centroid positions. Bar, 5 μm.

fluorescence intensity (see also Figures 2A and 2B) likely due to the presence of actin-based ruffling and increased volume near the central-peripheral domain boundary.

F-Actin Flow Patterns under Control Conditions

Before investigating changes in F-actin flow during target interactions, it was essential to characterize the temporal and spatial variation of retrograde flow rates throughout growth cone lamellae. To do so, we systematically compared flow-coupled bead movements within different regions of the growth cone. Beads were positioned on the lamella using the laser tweezers, and translocation rates were plotted as a function of the angle (α) of bead movements relative to a reference line parallel to the long axis

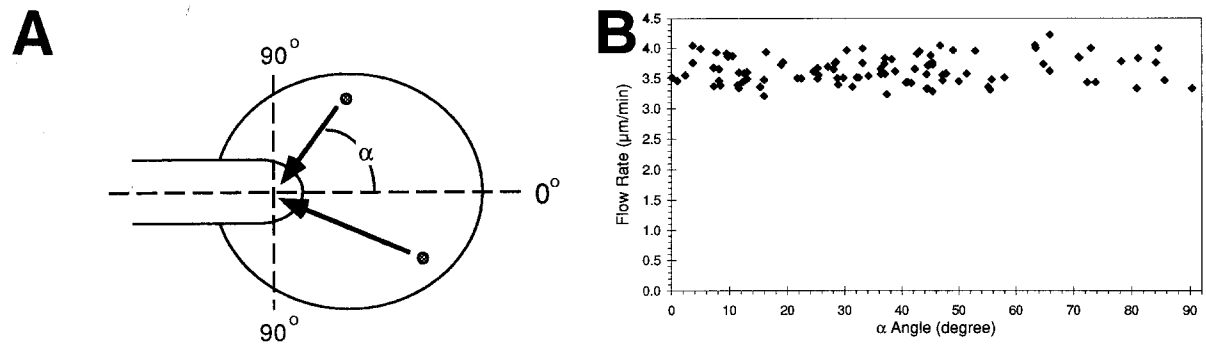

Figure 4. F-Actin Flow in Isolated Growth Cone Lamella Is Isotropic

(A) Flow-coupled beads were applied to the entire growth cone lamella using laser tweezers. Rates of retrograde F-actin flow were estimated by rates of bead transport at varying angles (α) of bead movement relative to a reference line parallel to the long axis of the neurite and through the approximate center of the growth cone.

(B) A representative pattern of F-actin flow in an isolated growth cone. Average translocation rates of individual beads over a 100 s interval were plotted as a function of angle of bead movement (α). A total of 102 bead measurements were made on this growth cone.

and through the approximate center of the growth cone (Figure 4A). A representative flow versus angle plot is shown in Figure 4B. Note that retrograde flow rates appear to be spatially isotropic throughout the peripheral lamella (4.95 ± 0.30 μm/min, mean ± SD). Temporal variation of flow rate was also assessed at constant α by repeatedly positioning beads at the same distal starting location using the laser tweezers. Over an observation period of 30 min, local flow rates fluctuated less than 10% (4.91 ± 0.29 μm/min at $\alpha \leq 5$, mean ± SD; see also Forscher and Smith, 1988).

F-Actin Flow Patterns during Target Interactions

Using flow-coupled beads as a tool to monitor F-actin movements, F-actin flow maps before and during growth cone-target interactions were generated by quickly placing beads at desired positions on the growth cone surface using the laser tweezers. Before observable central domain extension, beads in the growth cone–target interaction corridor exhibited control rates of retrograde flow (line in Figure 5A). When the central domain began to move rapidly forward toward the target site (i.e., growth cone–target coupling; see Lin and Forscher, 1993), the bead located along the interaction axis exhibited little or no retrograde movement (line in Figure 5B). Coordinate movement of the leading edge (open squares), the on-axis bead (open circles), and the central domain (closed squares) of the lower growth cone in Figure 5B is plotted over time in Figure 5C. Note that the progressive slowing of the on-axis bead in the initial 100 s time interval was accompanied by an increase in the rate of central domain extension. By about the 120 s time point (arrowheads in Figures 5B and 5C), the on-axis bead had stopped moving in the retrograde direction, and the central domain had reached its maximum rate of extension (3.30 μm/min). Note that this rate of extension approaches the actin flow rate measured before the interaction took place (3.42 μm/min) and also that leading edge advance was correlated with that of the central domain.

To determine whether the slowing of retrograde flow occurred specifically along the interaction axis, beads were placed either along the interaction axis or off axis by $\geq 40°$ to monitor F-actin flow simultaneously in both domains during an interaction (Figure 6A). The bead positioned outside the interaction corridor (Figure 6B) continued to exhibit retrograde movement at control rates throughout the recording. In contrast, retrograde movement of the on-axis bead slowed (Figure 6C) when central domain extension was observed. Comparison of displacement plots for both beads (Figure 6D) shows that the on-axis bead (open circles) moved at about half the rate of the off-axis bead (closed circles). Note that in this experiment, retrograde movement of the on-axis bead never stopped completely (maintained 43% of the control flow rate) and the central domain (closed squares) exhibited only a moderate rate of forward advance (about 60% of the control flow rate). It is noteworthy to contrast this behavior with that in Figure 5, in which the on-axis bead stopped completely, and the rate of central domain advance was correspondingly greater (96%), approaching the rate of retrograde flow.

Retrograde Flow Is Inversely Proportional to Growth Cone Advance

It appeared from these experiments that during target interactions, slower rates of on-axis bead transport were correlated with faster rates of both central domain and leading edge advance. Leading edge movements were usually characterized by transient protrusions and retractions and sometimes obscured altogether by ruffling and/or organelles near the site of interaction (e.g., Figure 6C). In contrast, central domain movement was more or less monotonic and as a result could be assessed with greater precision. We therefore examined the correlation between on-axis flow rates and rates of central domain extension, using the latter as an indicator of growth cone advance. Data from many interactions was pooled by normalizing the rate of central domain extension (R_{cen}) and the transport rate of on-axis beads ($R_{on\text{-}axis}$) by control retrograde flow rates (R_{flow}) measured in individual growth cones. Note that $R_{on\text{-}axis}$ and R_{cen} reflect average velocities obtained during periods of central domain extension (typically $\geq$60 s in duration). When normalized R_{cen} was plotted as a func-

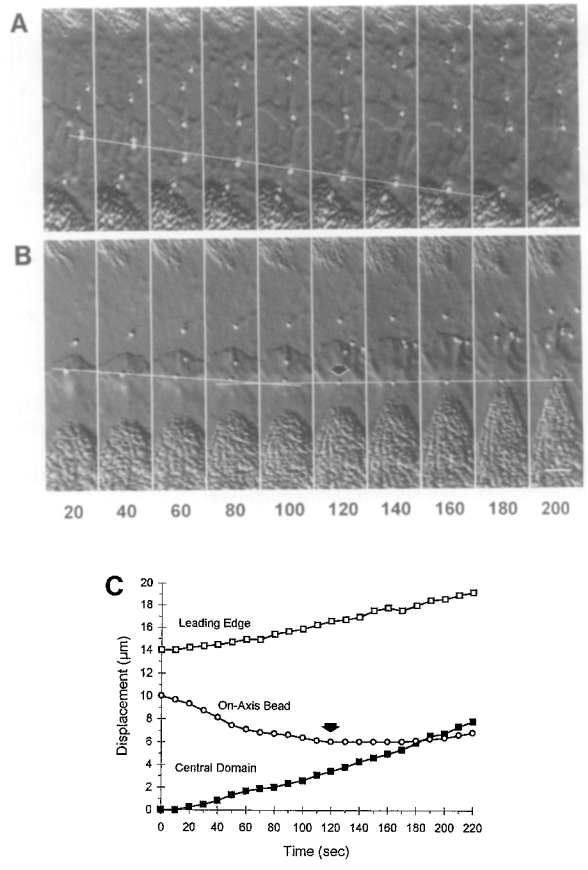

Figure 5. Attenuation of F-Actin Flow during a Growth Cone–Target Interaction

(A) Beads exhibit clear retrograde movement (line) after contact with target but before central domain extension (i.e., before target coupling).

(B) Retrograde movement of the bead (line) along the target interaction axis was attenuated when the central domain began to extend rapidly toward the target contact site. Note the leading edge of the lower growth cone advances in parallel with central domain. Time intervals between images are 20 s; bar, 5 μm.

(C) Cumulative displacement of the central domain (closed squares), the leading edge (open squares), and centroid position of the on-axis bead (circles) plotted as a function of time for the interaction shown in (B). Positive numbers denote anterograde movement. Note that in the first 100 s, the on-axis bead exhibits some retrograde movement while extension of the central domain is slow. By the 120 s time point (arrowheads in [B] and [C]), retrograde flow is nearly zero, and the central domain begins rapid extension.

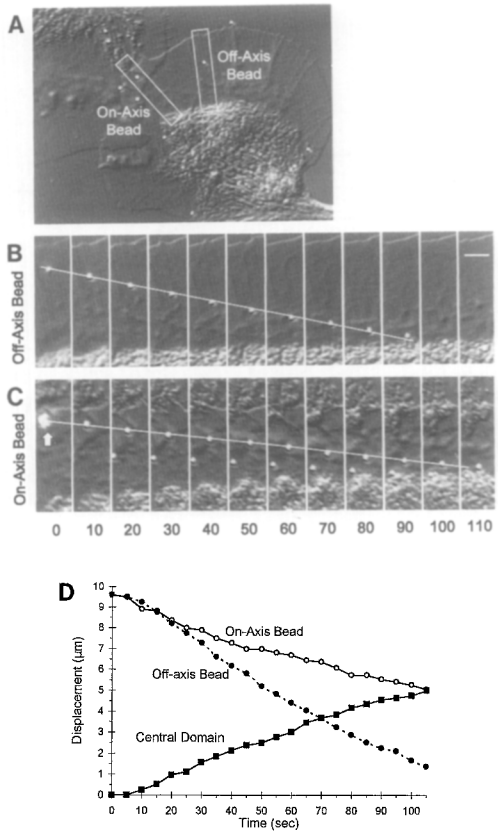

Figure 6. Retrograde F-Actin Flow Is Attenuated Specifically along the Target Interaction Axis

(A) Laser tweezers were used to position beads at specific sites, either along the target interaction axis (on-axis bead) to measure the axial flow rate ($R_{on\text{-}axis}$) or ⩾40° off axis (off-axis bead) to assess F-actin movements (R_{flow}) during target interactions. Bar, 10 μm.

(B) Image sequence of the off-axis bead movement (line). Note that the bead was internalized at the central domain.

(C) Time sequence of on-axis bead movement (line) and central domain advance along the interaction axis. The arrow points to a bright spot caused by reflection of infrared light from the laser tweezers used to position bead. Clear identification of the leading edges of the interacting growth cones, in this experiment, was obscured by ruffling at the site of interaction.

(D) Displacement of on-axis bead (open circles), off-axis bead (closed circles), and central domain (closed squares) as a function of time. Note that retrograde motion of the on-axis bead (2.24 μm/min) is substantially slower than off-axis bead (5.18 μm/min) and moderate rate of central domain extension (3.11 μm/min).

tion of $R_{on\text{-}axis}$, an inverse relationship was readily apparent (Figure 7; data from 23 interactions; slope of least squares fit line = −0.97), showing that the rate of directed central domain extension, and by inference, microtubule extension (Bridgman et al., 1986; Forscher and Smith, 1988), was inversely proportional to the rate of retrograde F-actin flow in situ.

Discussion

Surface Marker Movement Reflects F-Actin Flow

In the present study, we have investigated changes in retrograde F-actin flow during growth cone–target interactions. To monitor the flow noninvasively, we first demonstrated experimental conditions under which membrane-bound beads coupled reliably to intracellular actin networks, allowing bead movements to be used to monitor the underlying F-actin flow (see Figure 3). In a recent study, different rates were reported for retrograde flow and movement of extracellular particles or surface features in fibroblast lamellae (Theriot and Mitchison, 1992). The nature of this apparent disparity remains unclear and may result from differences in cell type or in the assays employed. Note, however, that we have previously reported conditions for Aplysia neurons under which membrane-bound beads do not maintain a strictly flow-coupled state. For

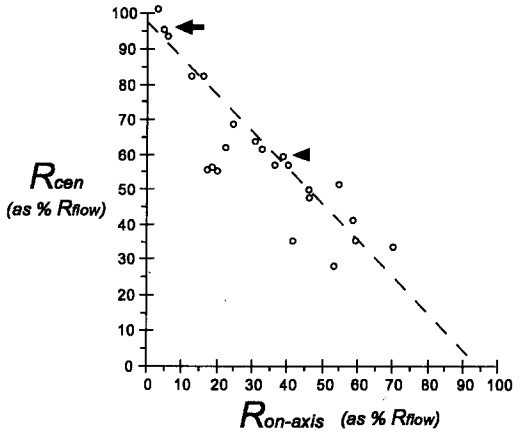

Figure 7. The Rate of Central Domain Extension Is Inversely Proportional to the Rate of Retrograde F-Actin Flow

Each point represents one growth cone–target interaction; data pooled from 23 different experiments are shown. Rates of central domain extension (R_{cen}) and rates of flow-coupled bead movement along the target interaction axis ($R_{on\text{-}axis}$) were normalized by retrograde flow rates (R_{flow}) measured in each individual growth cone. Data from interactions shown in Figure 5 and Figure 6 are indicated by arrow and arrowhead, respectively.

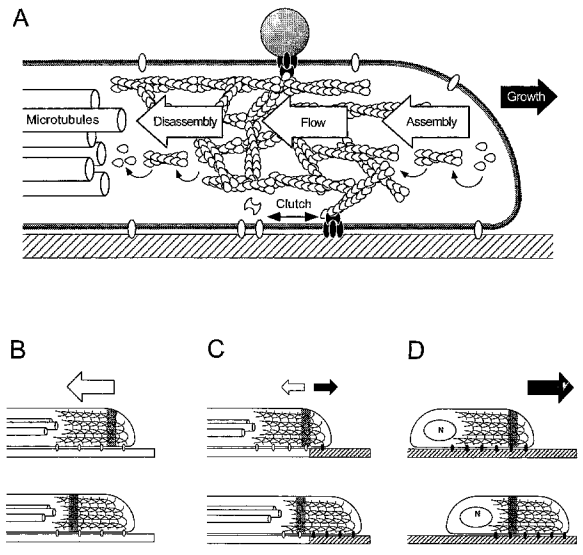

Figure 8. Substrate–Cytoskeletal Coupling Motility Model

(A) Actin dynamics of a neuronal growth cone lamellipodium represented by a steady state composed of three superimposed kinetic processes (open arrows): net F-actin assembly along the leading edge, net F-actin disassembly, and retrograde F-actin flow at a rate matching assembly and disassembly. "Clutch" protein complexes may modulate the degree of mechanical coupling between intracellular F-actin and external substrates (double-headed arrow).

(B, C, and D) Spectrum of cell motility observed under conditions of increasing F-actin–substrate coupling efficiency. Reference marks in F-actin indicated by stippled bars. Membrane–cytoskeletal "clutch" protein complexes are shown either uncoupled or coupled to external substrates by open and closed ovals, respectively.

(B) A representation of Aplysia growth cones plated on a nonpermissive growth substrate (unshaded) where robust retrograde F-actin flow (large open arrow) and little leading edge advance is observed.

(C) When growth cone encounters a permissive growth substrate (hatched) boundary, the retrograde flow becomes attenuated (small open arrow), and the rate of growth cone advance increases (closed arrow).

(D) In contrast, rapidly migrating cells like fish keratocytes exhibit virtually no retrograde actin flow relative to the substrate and advance at nearly the rate of actin filament assembly (large closed arrow).

example, when beads are derivatized with polycationic agents exhibiting high membrane adhesivity, nonlinear bead movements are observed that are associated with the formation of F-actin tails. These bead movements appear to derive their motive force from actin filament assembly and have been shown to be kinetically independent of retrograde actin flow (Forscher et al., 1992). On the other hand, under conditions promoting weak bead–membrane interactions, beads tend to exhibit limited diffusion and retrograde drift (C.-H. L, C. A. Thompson, and P. F., unpublished data). In both these cases, bead trajectories and velocities clearly do not reflect retrograde F-actin flow dynamics accurately. To use beads as a tool to study F-actin dynamics, care was taken to maintain beads strictly in the actin flow-coupled state (see Experimental Procedures).

Retrograde F-Actin Flow Patterns

The photobleaching (see Figure 3) and actin flow mapping (see Figure 4) experiments suggest that under control conditions, the entire lamellar F-actin domain exhibits a spatially uniform pattern of retrograde flow in accord with previous pharmacological studies (Forscher and Smith, 1988). In support, no significant irregularities in the movement of photobleached F-actin marks, such as splitting, bending (Lee et. al., 1993), or widening, were observed, as would be expected if multiple F-actin domains (Lewis and Bridgman, 1992) moving at significantly different rates were present. It is possible, however, that signal-to-noise limitations in the present system would not have permitted us to detect the presence of a small population of actin filaments with different kinetic properties. Further studies will be necessary to address this particular issue.

The uniform pattern of the retrograde flow was perturbed during growth cone–target interactions; specifically, rates of retrograde flow-coupled bead movement were attenuated in a spatially restricted corridor parallel to the target interaction axis. One possible explanation for this slowing of on-axis bead movement is that coupling of beads to underlying F-actin was reduced along the interaction axis. We consider this scenario unlikely since beads not anchored to the actin cytoskeleton typically exhibit Brownian motion easily detected in real-time observations. During interactions, bead diffusion was very limited, if present at all; thus, the observed slowing of on-axis bead movement more likely reflects attenuation of the underlying F-actin flow. Retrograde flow was also found to be inversely proportional to the rate of growth cone advance (Figure 7) over a wide range of flow and advance rates. The graded nature of this inverse relationship suggests a mechanism by which rates of growth cone advance may be regulated by the degree of coupling between the intracellular actin cytoskeleton and extracellular target substrate, which will be considered below.

F-Actin–Substrate Coupling and Motility

Retrograde F-actin flow appears to be maintained in a steady state by superimposition of three distinct kinetic processes (Figure 8A): net filament assembly at the leading edge, retrograde movement of actin networks (at rates matching net assembly), and disassembly and/or severing of filaments at a proximal site (Forscher and Smith, 1988; Mitchison and Kirschner, 1988; Smith, 1988). How could perturbation of this steady state result in the observed changes in structure and motility during growth cone–target interactions? If growth promoting conditions result in more efficient coupling of intracellular actin networks to extracellular substrates, the increased number of F-actin–substrate linkages (Figure 8A, "Clutch") could lead to attenuation of retrograde F-actin flow proportional to the number of engaged clutch complexes formed. Note that in this model, slowing of the retrograde flow alone would result in anterograde flux of both the leading edge and proximal F-actin boundary (assuming continued actin assembly and disassembly at respective sites; Figure 8C).

Why do microtubules move rapidly toward the target interaction site? One possible explanation is that anterograde movement of the proximal F-actin boundary simply removes steric restraints imposed on microtubules by peripheral F-actin networks. This mechanism is supported by a previous report that depletion of peripheral F-actin subsequent to cytochalasin treatment resulted in rapid microtubule extension (Forscher and Smith, 1988). Whether this microtubule redistribution actually involves plus end–directed assembly (Bamburg et al., 1986; Tanaka and Kirschner, 1991) or a microtubule sliding mechanism (Koonce et al., 1987; Cleveland and Hoffman, 1991; Joshi and Baas, 1993) is not known. Microtubule extension might alternatively result from microtubule interactions with actomyosin complexes; however, until the putative myosins involved in growth cone motility have been better characterized, such mechanisms remain speculative.

What is the relationship between leading edge and central cytoplasmic domain advance? Tracking the position of the leading edge during interactions was often difficult, owing to the presence of both ruffling and organelles at interaction sites (e.g., see Figure 6). In cases in which the leading edge was readily discernible (e.g., see Figure 5), its advance correlated well with that of the central domain. An exception to this rule was sometimes observed during the initial phase of a target interaction, when the rate of leading edge advance appeared to be slower than that of the central domain (see Figure 1). Active ruffling characterized by vertical protrusions is always present at target interaction sites during this initial phase; the higher frequency of vertical versus forward protrusions may account for the lag in leading edge advance. Alternatively, the delay could reflect changes in actin assembly rates or other unknown signaling events necessary to trigger leading edge advance. At later time points, after growth cones had moved off of the poly-L-lysine on to native neuronal substrates, both the leading edge and the central domain sustained faster rates of advance (see Figure 1B after 10 min) compared to those before the interaction. It will be interesting to see whether the inverse relationship between retrograde flow and growth cone advance rates will hold true when extended to other physiological substrates and different neuronal subtypes in the future.

What general implications do these results have for cell motility? The observation that the rate of growth cone advance is inversely proportional to retrograde F-actin flow (see Figures 5–7) suggests that a continuum of substrate–cytoskeleton coupling efficiency levels exists that may correspond to different degrees of directed motility. In growth cones and slowly moving cells, F-actin assembled at the leading edge is transported centripetally by the retrograde flow (large open arrow in Figure 8B), apparently without significant substrate coupling (Wang, 1987; Forscher and Smith, 1988; Okabe and Hirokawa, 1991). On the other hand, in more rapidly migrating cells, the rate of leading edge advance is about equal to the rate of actin filament assembly (large closed arrow in Figure 8B), and these cells exhibit little or no retrograde F-actin flow relative to the substrate (Theriot and Mitchison, 1991), suggesting more efficient actin–substrate coupling. When a neuronal growth cone interacts with a favorable target substrate (Lin et al., 1994; Figure 8C), its rate of advance appears to increase (closed arrow) in direct proportion to the degree of attenuation of retrograde actin flow (open arrow); however, to match typical retrograde flow rates, axonal growth would have to proceed at 180–360 μm/hr, rates significantly higher than those observed in vivo and in vitro (Mason, 1985). This implies that maximum rates of growth cone advance (i.e., those predicted by complete attenuation of retrograde flow) probably occur only transiently under physiological conditions. Thus, even on the most favorable substrates, growth cones likely experience some degree of clutch slippage.

Experimental Procedures

Cell Culture and Video Microscopy

Cell culture and video microscopy techniques were performed as previously described (Forscher and Smith, 1988; Lin and Forscher, 1993).

Fluorescent Labeling of Actin Proteins

Actin proteins were prepared from chicken skeletal muscle and labeled with tetramethylrhodamine-5-iodoacetamide (IATR; Molecular Probe, Eugene, OR) according to the protocol of Wang (1985) with some modification (personal communication with Dr. Yu-Li Wang). In brief, 5 mg/ml monomeric actin in buffer 1 (0.5 mM ATP, 0.2 mM $CaCl_2$, 2 mM Tris-HCl [pH 8.0]) was first polymerized by adding 100 mM KCl and 2 mM $MgCl_2$. IATR was dissolved in dimethyl sulfoxide (DMSO) then added to an aqueous solution (100 mM KCl, 100 mM boric acid [pH 8.0]). The dye slurry was clarified by centrifugation and added to the F-actin solution at 1:1 molar ratio. After 2 hr incubation at 4°C, the reaction was stopped by adding dithiothreitol to a final concentration of 10 mM, then dialyzed against buffer 1. The resulting G-actin solution was passed through a G-25 gel filtration column to get rid of residual dyes, then purified by another polymerization–depolymerization cycle. Typical labeling reactions resulted in calculated dye/protein molar ratios of 0.8–1.1. The labeled G-actin was drop-frozen in liquid nitrogen and stored at −80°C until use.

Labeling F-Actin with RH-Ph

RH-ph microinjection protocol was a modification of Wang (1987). In brief, 150 μl of 3.3 μM RH-ph methanol solution (Molecular Probes, Eugene, OR) was dried with nitrogen, redissolved in 0.5 μl of DMSO, then diluted with 4.5 μl injection buffer (100 mM K–aspartate, 10 mM HEPES [pH 7.6]); this reagent was made fresh before microinjection.

Microinjection and Photobleaching

Bag cell neurons were transferred to a custom-made injection chamber; then the cell bodies were impaled with a glass pipette mounted on a piezoelectric axial drive (Burleigh Instruments, Fishers, NY). Typically, less than 10% cell volume of labeling reagent or vehicle solution was injected. Given the amounts of RH-ph injected, we estimated that actin filaments were labeled at a stoichiometry of about 1:10. After microinjection, cells were incubated for at least 2 hr at room temperature before photobleaching experiments. A Bio-Rad 500 confocal microscope (Bio-Rad, Richmond, CA) was used for simultaneous DIC and fluorescent observations. After applying positively charged polystyrene beads to the cells, photobleached marks were made by high power single line scans near the site of bead attachment. Paired DIC–fluorescence images were then recorded using a 10 s sampling interval. Kinetic analysis was done using programs developed in this laboratory (Forscher et al., 1992; Lin and Forscher, 1993).

Surface Markers

To prepare polycationic beads for this study, polystyrene beads (500 nm; Polyscience, Warrington, PA) were first coated with polyethyleneimine (Forscher and Smith, 1990) and then incubated for 10 min with culture medium supplemented with 10 mg/ml bovine serum albumin before application to cells to inhibit possible triggering of subjacent F-actin assembly by beads (inductopodia formation; Forscher et al., 1992). In addition, all experiments were performed in the constant presence of bovine serum albumin to ensure that beads remained in the actin flow-coupled state.

Micropositioning

Laser tweezers were used to position beads critically during target interactions recorded using time-lapse video-enhanced DIC microscopy. The laser trap employed a 40 mW laser diode emitting at 790 nm as a light source. Details of laser trap construction will be reported elsewhere.

Acknowledgments

We wish to thank Dr. Y.-L. Wang for advice on actin labeling, Drs. M. Mooseker, R. Cheney, W. Bement, L. Errante, and C. Thompson for comments and discussion, and Drs. L. Cramer and T. Mitchison for providing labeled actin for pilot experiments. This work was supported by National Institutes of Health grant RO1-NS28695 and a McKnight Endowment Fund Award to P. F. and a scholarship from the Education Department of Taiwan to C.-H. L.

The costs of publication of this article were defrayed in part by the payment of page charges. This article must therefore be hereby marked *"advertisement"* in accordance with 18 USC Section 1734 solely to indicate this fact.

Received August 2, 1994; revised January 1, 1995.

References

Bamburg, J. R., Bray, D., and Chapman, K. (1986). Assembly of microtubules at the tips of growing axons. Nature *321*, 788–790.

Block, S. M. (1990). Noninvasive Techniques in Cell Biology. (New York: Wiley-Liss), pp. 375–401.

Bray, D., White J, G., Bray, D., and White, J. G. (1988). Cortical flow in animal cells. Science *239*, 883–888.

Bridgman, P. C., Kachar, B., and Reese, T. S. (1986). The structure of cytoplasm in directly frozen cultured cells. II. Cytoplasmic domains associated with organelle movement. J. Cell Biol. *102*, 1510–1512.

Burmeister, D. W., Rivas, R. J., and Goldberg, D. J. (1991). Substrate-bound factors stimulate engorgement of growth cone lamellipodia during neurite elongation. Cell Motil. Cytoskeleton *19*, 255–268

Cleveland, D. W., and Hoffman, P. N. (1991). Slow axonal transport models come full circle: evidence that microtubule sliding mediates axon elongation and tubulin transport. Cell *67*, 453–456.

Cypher, C., and Letourneau, P. C. (1992). Growth cone motility. Curr. Opin. Cell Biol. *4*, 4–7.

Forscher, P., Lin, C.-H., and Thompson, C. (1992). Novel form of growth cone motility involving site-directed actin filament assembly. Nature *357*, 515–518.

Forscher, P., and Smith, S. J. (1988). Actions of cytochalasins on the organization of actin filaments and microtubules in a neuronal growth cone. J. Cell Biol. *107*, 1505–1516.

Forscher, P., and Smith, S. J. (1990). Cytoplasmic actin filaments move particles on the surface of a neuronal growth cone. In Optical Microscopy for Biology. (New York: Wiley-Liss), pp. 459–471.

Goodman, C. S., and Shatz, C. J. (1993). Developmental mechanisms that generate precise patterns of neuronal connectivity. Cell *72*/Neuron *10* (Suppl.), 77–98.

Hatten, M. E. (1993). The role of migration in central nervous system neuronal development. Curr. Opin. Neurobiol. *3*, 38–44.

Heidemann, S. R., Lamoureux, P., and Buxbaum, R. E. (1991). On the cytomechanics and fluid dynamics of growth cone motility. J. Cell Sci. (Suppl.) *15*, 35–44.

Joshi, H. C., and Baas, P. W. (1993). A new perspective on microtubules and axon growth. J. Cell Biol. *121*, 1191–1196.

Kaczmarek, L. K., Finbow, M., Revel, J. P., and Strumwasser, F. (1979). The morphology and coupling of Aplysia bag cells within the abdominal ganglion and in cell culture. J. Neurobiol. *10*, 525–550.

Koonce, M. P., Tong, J., Euteneuer, U., and Schliwa, M. (1987). Active sliding between cytoplasmic microtubules. Nature *328*, 737–739.

Lander, A. D. (1992). Contact and adhesive specificities in the associations, migrations, and targeting of cells and axons. Cell *68*, 303–322.

Lee, J., Ishihara, A., Theriot, J. A., and Jacobson, K. (1993). Principles of locomotion for simple shaped cells. Nature *362*, 167–171.

Letourneau, P. C., Condic, M. L., and Snow, D. M. (1994). Interactions of developing neurons with the extracellular matrix. J. Neurosci. *14*, 915–928.

Lewis, A. K., and Bridgman, P. C. (1992). Nerve growth cone lamellipodia contain two populations of actin filaments that differ in organization and polarity. J. Cell Biol. *119*, 1219–1243.

Lin, C.-H., and Forscher, P. (1993). Cytoskeletal remodeling during growth cone-target interactions. J. Cell Biol. *121*, 1369–1383.

Lin, C.-H., Thompson, C. A., and Forscher, P. (1994) Cytoskeletal reorganization underlying growth cone motility. Curr. Opin. Neurobiol. *4*, 640–647.

Mason, C. (1985). How do growth cones grow? Trends Neurosci. *8*, 304–306.

Mitchison, T., and Kirschner, M. (1988). Cytoskeletal dynamics and nerve growth. Neuron *1*, 761–772.

O'Connor, T. P., and Bentley, D. (1993). Accumulation of actin in subsets of pioneer growth cone filopodia in response to neural and epithelial guidance cues in situ. J. Cell Biol. *123*, 935–948.

O'Leary, D. D. M., and Koester, S. E. (1993). Development of projection neuron types, axon pathways, and patterned connections of mammalian cortex. Neuron *10*, 991–1006.

Okabe, S., and Hirokawa, N. (1991). Actin dynamics in growth cones. J. Neurosci. *11*, 1918–1929.

Smith, C. L. (1994). Cytoskeletal movements and substrate interactions during initiation of neurite outgrowth by sympathetic neurons in vitro. J. Neurosci. *14*, 384–398.

Smith, S. J. (1988). Neuronal cytomechanics: the actin-based motility of growth cones. Science *242*, 708–715.

Tanaka, E. M., and Kirschner, M. W. (1991). Microtubule behavior in the growth cones of living neurons during axon elongation. J. Cell Biol. *115*, 345–363.

Theriot, J. A., and Mitchison, T. J. (1991). Actin microfilament dynamics in locomoting cells. Nature *352*, 126–131.

Theriot, J. A., and Mitchison, T. J. (1992). Comparison of actin and cell surface dynamics in motile fibroblasts. J. Cell Biol. *119*, 367–377.

Wang, Y. (1985). Exchange of actin subunits at the leading edge of living fibroblasts: possible role of treadmilling. J. Cell Biol. *101*, 597–602.

Wang, Y. L. (1987). Motility of filamentous actin in living cytoplasm. J. Cell Biol. *105*, 2811–2816.